Biosensors and Bioelectronics 124–125 (2019) 15–24

Contents lists available at ScienceDirect

Biosensors and Bioelectronics

journal homepage: www.elsevier.com/locate/bios

A versatile signal-enhanced ECL sensing platform based on molecular imprinting technique via PET-RAFT cross-linking polymerization using bifunctional ruthenium complex as both catalyst and sensing probes

Jintao Cai[a,1], Tao Chen[a,1], Yuanhong Xu[b], Shuang Wei[a], Weiguo Huang[a], Rui Liu[a], Jingquan Liu[a,*]

[a] College of Materials Science and Engineering; Institute for Graphene Applied Technology Innovation; State Key Laboratory of Biopolysaccharide Fibers and Ecological Textiles, Qingdao University, Qingdao 266071, China
[b] College of Life Sciences, Qingdao University, Qingdao 266071, China

ARTICLE INFO

Keywords:
Molecular imprinted polymers
Electrochemiluminescence (ECL)
PET-RAFT cross-linking polymerization
Melamine
$Ru(bpy)_3^{2+}$

ABSTRACT

Molecularly imprinted technique (MIT) has proven to be a significant tool in the analyzing area in virtue of its obvious advantages such as specific recognition, favorable stability to high temperature and higher sensitivity. Electrochemiluminescence (ECL) technology has also been receiving enormous attention as a powerful tool in sensing fields. However, sensors based on the combination of MIT and ECL technologies have seldom been reported yet. Herein, we find that $Ru(bpy)_3^{2+}$ cannot only work as an efficient catalyst for photo-induced electron transfer–reversible addition–fragmentation chain transfer (PET-RAFT) polymerization, but also as a sensing probe for ECL sensor. Based on this, we successfully construct ECL sensors via the combination of MIT and ECL techniques. In details, poly(methacrylic acid) (PMAA) and cross-linked PMAA were synthesized first via a well-controlled PET-RAFT polymerization using $Ru(bpy)_3^{2+}$ as catalyst under illumination of visible light with a wavelength of 460 nm, as confirmed by ^1H NMR and gel permeation chromatography (GPC). Then, negatively-charged Au nanoparticles (AuNPs) with average sizes of 20 nm were prepared and modified with $Ru(bpy)_3^{2+}$ via electrostatic incorporation. MIPs were prepared on the surface of AuNPs using melamine (MEL) as the template via PET-RAFT controlled cross-linking polymerization. The MIPs modified AuNPs (AuNPs-MIPs) were then fixed on the surface of working electrode with Nafion to achieve a solid-state ECL sensing platform employing $Ru(bpy)_3^{2+}$ as the ECL probes. The as-prepared sensor showed a wide detection range of $5.0 \times 10^{-13} - 5.0 \times 10^{-6}$ mol/L and a low detection limit of 1.0×10^{-13} mol/L (S/N ≥ 3) was reached in the detection of MEL. Moreover, further tests for analyzing MEL structural analogues proved that the constructed ECL sensing platform could be utilized to detect various substances via specific recognitions.

1. Introduction

Molecular imprinted polymers (MIPs) (Cakir et al., 2013; Chen et al., 2016a; Schirhagl, 2014; Uzun and Turner, 2015) have rapidly gained enormous interest owning to their broad applications in chemical sensing (Gomez et al., 2016; Li et al., 2013), separation (He et al., 2014), drug delivery (Yin et al., 2010), and extraction (Cai et al., 2014b). In the presence of a certain molecule template, MIPs can be synthesized by copolymerization of the functional monomers and cross-linking agents. The function of cross-linking agent is to stabilize the recognition sites after removal of the template molecules, leaving the MIPs with recognition cavities for the detection of molecular analytes with similar structures. (Chen et al., 2011) Compared to other assay techniques, MIPs own many significant characteristics, such as specific recognition and high stability to high temperatures (Li et al., 2014). However, the cross-linking polymerization process of MIPs usually needs higher temperature, various initiators or catalysts, which could restrict their potential bio-applications (Chen et al., 2011) and increase the complexity of purification. Therefore, facile and gentle polymerization methods are urgently needed for the preparation of MIPs.

Photo-induced electron transfer–reversible addition–fragmentation chain transfer (PET-RAFT) polymerization (Cao et al., 2015; Fu et al., 2014; Tao et al., 2017; Xu et al., 2014), as a kind of gentle synthetic technique initiated by visible light in the presence of photocatalyst at room temperature, is an appropriate method for the polymerization of MIPs using biological materials as the templates. Therein, $Ru(bpy)_3^{2+}$

* Corresponding author.
E-mail address: jliu@qdu.edu.cn (J. Liu).
[1] Jintao Cai and Tao Chen contributed equally to this work.

https://doi.org/10.1016/j.bios.2018.09.083
Received 2 June 2018; Received in revised form 12 September 2018; Accepted 24 September 2018
Available online 25 September 2018
0956-5663/

has been confirmed to be an effective photocatalyst for RET-RAFT polymerization. (Chen et al., 2018a; Tao et al., 2017) It is noteworthy that $Ru(bpy)_3^{2+}$ is also a kind of typical electrochemiluminescence (ECL) reagent in the fabrication of ECL sensors. (Feng et al., 2017; Zhang et al., 2017) Compared with other sensing approaches such as high performance liquid chromatography (Chester, 2013), colorimetric assays (Ai et al., 2009), surface enhanced Raman spectroscopy (Xu et al., 2015), enzyme-linked immunoassays (Wang et al., 2010), mass spectrometry (Gillette and Carr, 2013) etc., ECL sensors (Miao et al., 2011; Nasiri and Sun, 2017) show some unique advantages such as simple operation, wider detection range and higher sensitivity. (Miao, 2008) In general, the detection principle of ECL sensors is based on the ECL coreactants which might obviously influence the ECL signals. (Xing et al., 2018) However, many ECL coreactants such as tripropylamine (Chen et al., 2018b), melamine (MEL (Liu et al., 2010a)) have similar effects on the ECL signals, which means the ECL sensors usually lack of specific recognition capability. Therefore, it could be anticipated that sensors based on the combination of MIPs and ECL techniques could be utilized for both MIPs and ECL sensing. Moreover, the simultaneous applications of the bi-functional $Ru(bpy)_3^{2+}$ in these two techniques could not only decrease the cost but also simplify the sensor fabrication procedures.

Till now, a large amount of works (Qian et al., 2014; Wei and Wang, 2008; Xu and Yu, 2010) have been carried out to explore the fixation of $Ru(bpy)_3^{2+}$ for the fabrication of solid-state ECL sensors in order to save the costly $Ru(bpy)_3^{2+}$ and strengthen the sensing stability. Many advanced materials such as graphene (Li et al., 2009), carbon nanotubes (Chen et al., 2009; Wu et al., 2013) and metal nanoparticles (Bertoncello and Forster, 2009; Guo et al., 2010; Lu et al., 2009) have been utilized for loading of more $Ru(bpy)_3^{2+}$ in order to increase the sensors' sensitivity. Among them, the sensors based on Au nanoparticles (AuNPs) showed better performance due to the good chemical and physical properties of AuNPs such as large specific surface area, excellent electrical conductivity and low toxicity (Wang et al., 2017; Zhao et al., 2014). Moreover, the electronegativity of AuNPs surface should benefit for the fixation of positive-charged $Ru(bpy)_3^{2+}$ via electrostatic adsorption (Chen et al., 2011). Besides, the localized surface plasmon resonance (LSPR) phenomenon of AuNPs could effectively increase the ECL intensity of $Ru(bpy)_3^{2+}$ which could apparently increase the sensitivity of the sensors. (Cheng et al., 2011; Nie et al., 2017; Wang et al., 2015b) Therefore, it could be anticipated that AuNPs could be an ideal substrate for the $Ru(bpy)_3^{2+}$ immobilization in the preparation of solid-state ECL sensors.

In present work, $Ru(bpy)_3^{2+}$-immobilized AuNPs (Ru-NPs) with average size of 20 nm were firstly prepared, followed by the generation of MIPs directly on the surface of AuNPs via $Ru(bpy)_3^{2+}$ catalyzed PET-RAFT (Ru-PET-RAFT) cross-linking polymerization using MEL as the template molecules. The MIPs modified AuNPs (AuNPs-MIPs) were fixed on the surface of working electrode by Nafion. (Miao, 2008; Zhang et al., 2009) Simultaneously, a sensitive solid-state ECL sensor (AuNPs-MIPs-HOPG) using $Ru(bpy)_3^{2+}$ as the ECL probes was successfully fabricated based on the combination of PET-RAFT polymerization, MIPs and ECL. The successful development of solid-state ECL sensor was confirmed by systematic characterizations using atomic force microscopy (AFM), energy dispersive spectroscopy (EDS), electrochemical impedance spectroscopy (EIS), cyclic voltammetry (CV) and ECL measurements. The experimental result indicated that the as-prepared ECL sensor had satisfied sensitivity, good reproducibility and excellent specific recognition in the detection of MEL.

2. Experimental section

2.1. Materials

Chloroauric acid ($HAuCl_4$, 99.9%) was obtained from Sigma-Aldrich (Steinheim, Germany). Trisoydium citrate dehydrate ($C_6H_5Na_3O_7{\cdot}2H_2O$, AR) was purchased from Sinopharm Chemical Reagent Co., Ltd. (Shanghai, China). Tris(2,2′-bipyridine) ruthenium dichloride ($Ru(bpy)_3Cl_2{\cdot}6H_2O$, 98.0%) was purchased from Ailan Chemical Technology Co., Ltd. (Shanghai, China). Methacylic acid (MAA, 99.0%) was obtained from Bodi Chemical Co., Ltd. (Tianjin, China). Dicyandiamide (99.5%), ammelide (99.5%) and cyanuric acid (99.5%) were obtained from Dingshengxin Chemical Industry Co., Ltd. (Tianjin, China). Ethylene glycol dimethacrylate (EGDMA, 98.0%), as a cross-linking agent, was bought from Aladdin Chemistry Co., Ltd. 2,2′-Azobis(isobutyronitrile) (AIBN) were obtained from Aladdin Chemistry Co., Ltd. The RAFT agent (4-Cyano-4-ethyl-trithiopentanoic acid (CETP)) was prepared according to the previous method. (Chen et al., 2016b; Liu et al., 2010b) The milk sample b was purchased from Mengniu Co., Ltd. (Neimenggu, China), sample c was purchased from Yili Co., Ltd. (Neimenggu, China), sample d was purchased from Bright Dairy & Food Co., Ltd. (Shanghai, China), sample e was purchased from Pinlive Food Co., Ltd. (Shanghai, China), sample f was purchased from Nestle (China) Co., Ltd. (Beijing, China), Sample a containing 0.15 mg/L MEL was obtained by addition of MEL into sample b. MEL (99.5%), an important industrial material in plastic engineering and agriculture that possesses high nitrogen content (66.0% by mass), (Wei et al., 2010) had been lawlessly doped in the dairy foods to increase the total nitrogen content on the basis of protein content measurements. (Cai et al., 2014a) It could endanger human reproductive system and urinary system via formation of kidney stones and other diseases. (Xu and Lu, 2015) Therefore, MEL was selected as the detecting target in our experiment. All reagents were used as received without further purification.

2.2. Apparatus

Infrared spectra were obtained on a PerkinElmer Spectrum One Fourier transform infrared (FTIR) spectroscope. The structure composition of poly(methacrylic acid) (PMAA) and cross-linked PMAA (cPMAA) were measured by a JNM-ECP 600 spectrometer, dimethyl sulphoxide (DMSO, 99.0%) and D_2O were used as deuterated solvents, respectively. Energy dispersive analysis (EDS) spectra were obtained from an EDS detector attached to the scanning electron microscope (SEM). Transmission electron microscope (TEM) measurements were carried out on a JEM-1200EX transmission electron microscopy operated at an accelerating voltage of 100 kV. AFM were carried out in tapping mode, the analytical approach of the obtained images was in virtue of WSxM software. Gel permeation chromatography (GPC) was used to calculate the relative molecular mass (Mn) and polydispersity index (Đ) of polymer, supported from a Shimadzu modular system. The CVs were measured using a CHI-760D electrochemical workstation (Shanghai, China). ECL experiments results were obtained by using a MPI-A ECL analyzer (Xi'an Remex Analytical Instrument, Co., Ltd, China), consisting of a dark chamber to collect the ECL response signal, with a photomultiplier tube window setting of 1000 V.

2.3. The preparation of PMAA via traditional RAFT polymerization

CETP (0.26 mg, 1.0×10^{-3} mmol), MAA (17.22 mg, 0.20 mmol) and AIBN (20 mg, 0.12 mmol) were dissolved in the mixture of DMSO (20 mL) and ultrapure water (5.0 mL) in a 50 mL round-bottom flask. The obtained mixture was purged for 30 min with ultrapure nitrogen gas, accompanied by stirring for 24 h at 75 °C in oil bath. Then, the obtained PMAA solution was dialyzed in diethyl ether three times before the desiccation treatment.

2.4. The preparation of PMAA via Ru-PET-RAFT polymerization

CETP (0.26 mg, 1.0×10^{-3} mmol), MAA (17.22 mg, 0.20 mmol) and $Ru(bpy)_3Cl_2{\cdot}6H_2O$ (2.0×10^{-2} mg, 2.7×10^{-6} mmol) were dissolved in a mixed solution of ethanol (20 mL) and ultrapure water

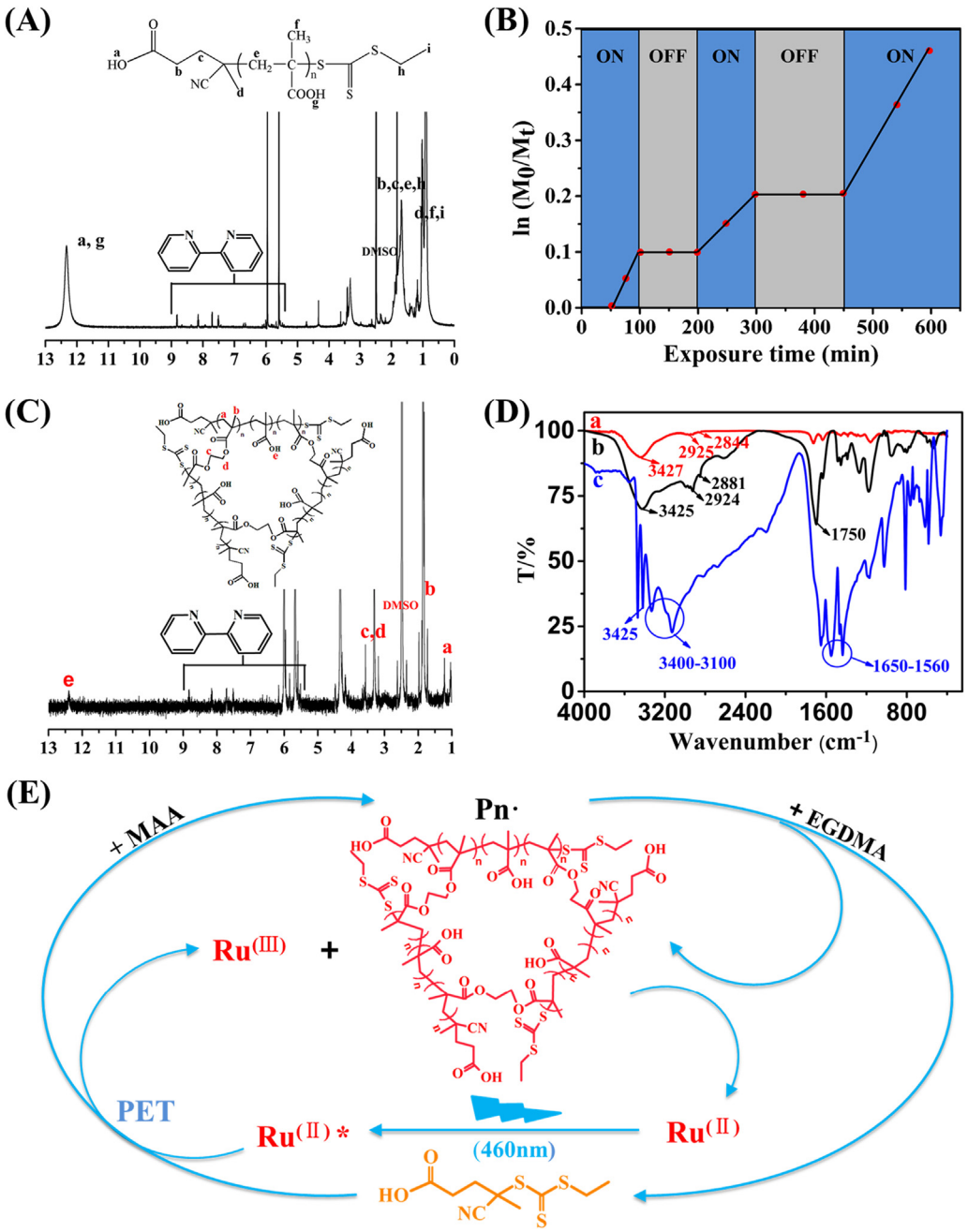

Fig. 1. (A) ^{1}H NMR spectra of the obtained PMAA via Ru-PET-RAFT polymerization. (B) "ON/OFF" control for Ru-PET-RAFT polymerization of MAA. (C) ^{1}H NMR spectra of the as-prepared cPMAA via Ru-PET-RAFT cross-linking polymerization. (D) FT-IR spectra of PMAA via traditional RAFT polymerization (a), PMAA via Ru-PET-RAFT polymerization (b) and cPMAA via Ru-PET-RAFT cross-linking polymerization (c). (E) Schematic illustration for the proposed mechanism of Ru-PET-RAFT cross-linking polymerization under visible light (λ = 460 nm) illumination at room temperature.

(5.0 mL) in a 50 mL flask. Then, the obtained solution was purged for 40 min with ultrapure nitrogen gas. Polymerization was carried out under the illumination of a blue light with a wavelength of 460 nm (165 W) under stirring and manipulated by adjusting the molar ratio of monomer to the RAFT agent as well as the polymerization time. Then, the obtained solution was purified by dialysis in ultrapure water for 3 days before desiccation treatment, afterwards characterized by ^{1}H NMR (Fig. 1A) and GPC. ^{1}H NMR (DMSO, 298 K, 600 MHz), δ (ppm from TMS): 12.40 (t, 1H, a), 8.60–5.50 ppm (pyridine groups), 1.60 (t, 2H, b), 1.00 (t, 3H, i).

2.5. The preparation of cPMAA via Ru-PET-RAFT cross-linking polymerization

CETP (0.26 mg, 1.0×10^{-3} mmol), MAA (17.22 mg, 0.20 mmol), EGDMA (198 mg, 1.0 mmol) and $Ru(bpy)_3Cl_2{\cdot}6H_2O$ (2.0×10^{-2} mg, 2.7×10^{-6} mmol) were dissolved in a mixture of ethanol (20 mL) and ultrapure water (5.0 mL) in a 50 mL flask. The obtained mixture was purged for 30 min with ultrapure nitrogen gas. Polymerization was carried out for 24 h under the light (460 nm) illumination at room temperature. Then, the obtained cPMAA was purified by dialysis in ultrapure water for 4 days before desiccation treatment and then characterized by ^{1}H NMR (As shown in Fig. 1C). ^{1}H NMR (DMSO, 298 K, 600 MHz), δ (ppm from TMS): 12.40 (d, 1H, e), 8.60–5.50 ppm

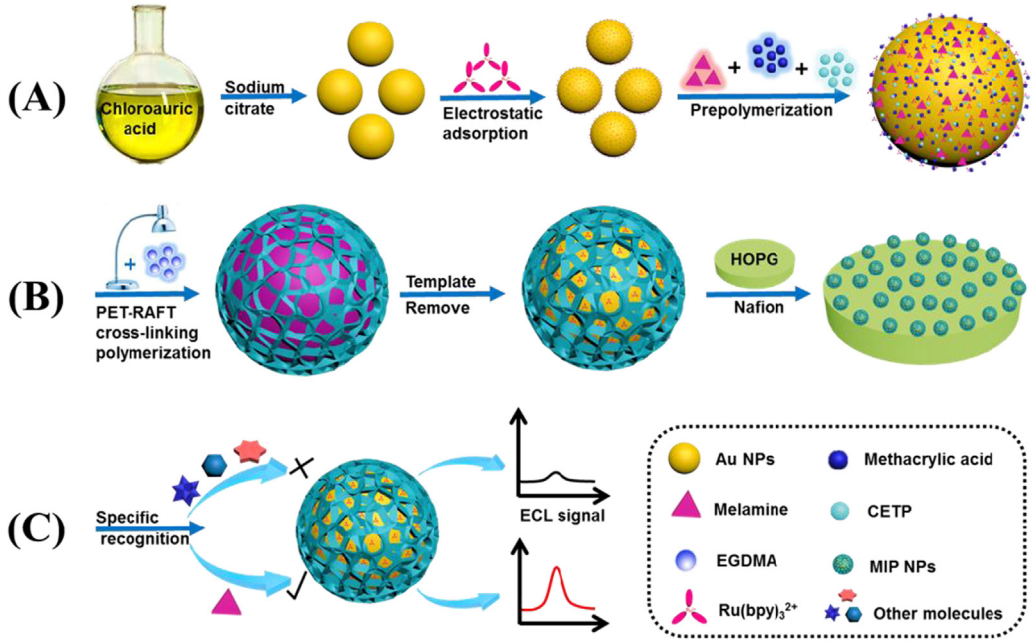

Scheme 1. (A) Schematic diagrams of the preparation procedure of $Ru(bpy)_3^{2+}$-immobilized AuNPs. (B) Preparation process of MEL-MIPs and ECL sensor. (C) The sensing tests via specific recognition using the as-prepared sensors.

(pyridine groups), 3.30 (t, 2H, c).

2.6. The preparation of Ru-AuNPs

The preparation process of Ru-AuNPs was illustrated in Scheme 1A and the detailed information was described as follows: The AuNPs were prepared according to the reported method. (Weissman et al., 2015) The detailed experimental process was shown as follows. Firstly, 50 mL ultrapure water was added into a 100 mL round-bottom flask, followed by the addition of 0.50 mL $HAuCl_4$ solution (1.0%). The obtained solution was then heated to a constant temperature at 95 °C and kept stirring for 30 min. Finally, 0.50 mL sodium citrate solution (1.0%) was added into the round bottom flask and let the reaction proceed for another 30 min 0.014 g $Ru(bpy)_3Cl_2{\cdot}6H_2O$ was added to 25 mL AuNPs (1.0 mg/mL) suspension and kept stirring at room temperature for 15 min to afford a large amount of black precipitation. Then, the product (Ru-AuNPs) was collected by centrifugation at 8000 rpm.

2.7. The preparation of MEL molecular imprinted polymers (Noted as MEL-MIPs)

MEL-MIPs were synthesized by Ru-PET-RAFT cross-linking polymerization, the whole process of the experiment is shown in Scheme 1B. The detailed information was described as follows: MEL (6.3 mg, 5.0×10^{-2} mmol) was completely dissolved in the mixture of ethanol (40 mL) and ultrapure water (10 mL) by sonication for 30 min. Then, MAA (17.22 mg, 0.20 mmol) was added to the obtained solution in ice bath. The resulting mixture was stirred for 6 h to afford the co-immobilization solution. EGDMA (198 mg, 1.0 mmol) and CETP (0.26 mg, 1.0×10^{-3} mmol), Ru-AuNPs (3.0 mL) were added to the above co-immobilization solution. After mixing by sonication for 10 min, the obtained mixture was purged for 30 min with pure nitrogen gas. Subsequently, Ru-PET-RAFT cross-linking polymerization was carried out for 24 h under the light (460 nm) illumination at room temperature. Finally, MEL-MIPs were obtained after dialysis in a mixed solvent of methanol and acetic acid (the volume ratio was 9:1) for 1 h to remove MEL. The preparation procedures of MIPs using MEL structural analogues such as dicyandiamide-MIPs and ammelide-MIPs were similar to those described above.

2.8. The preparation of non-molecular imprinted polymers (NIPs)

The NIPs was synthesized by a similar procedure to that of MIPs, but without adding the template molecules (MEL, dicyandiamide, ammelide and cyanuric) in the process of co-immobilization.

2.9. Fabrication of the solid-state ECL sensors (MEL-MIPs-HOPG and NIPs-HOPG)

12 mg MIPs (or NIPs) was added in the mixed solution of 0.25 mL ethanol (99.9%) and 0.25 mL Nafion (0.50 wt%). Before modification, HOPG was polished with alumina powder, rinsed with ultrapure water and dried in air. 60 μL of MIPs composite (or NIPs composite) was dripped onto the surface of the HOPG electrode, dried in air, and then the ECL sensors (MEL-MIPs-HOPG and NIPs-HOPG) were completely fabricated.

3. Results and discussion

3.1. The characterization of PMAA via Ru-PET-RAFT polymerization

PMAA was prepared via Ru-PET-RAFT polymerization under the visible light with the wavelength of 460 nm, the detailed synthesis process can be seen in Scheme 2A. The successful preparation of PMAA was proved by ^1H NMR. As shown in Fig. 1A, the peaks at 12.20 ppm should correspond to the carboxyl group from MAA and RAFT agent. The peaks at 8.90–5.50 ppm should be attributed to the pyridyl groups from $Ru(bpy)_3^{2+}$. The peaks at about 1.80 and 1.60 ppm should originate from the methylene groups and the peaks at 1.10–0.90 ppm should result from the methyl group, which indicate the presence of PMAA. Thanks to the electrostatic interaction between electropositive catalyst $Ru(bpy)_3^{2+}$ and the electronegative PMAA, the obtained solution is brownish red in color as shown in Scheme 2A(a), which is in agreement with the color of $Ru(bpy)_3Cl_2{\cdot}6H_2O$ (Fig. S1A). PMAA was also prepared by the traditional RAFT polymerization using AIBN as the initiator at 75 °C. As shown in Scheme 2B the water solution of PMAA is in light yellow (Scheme 2B(b)) which is mainly resulted from the yellow RAFT agent as shown in Fig. S1B.

In order to study the factors affecting the Ru-PET-RAFT

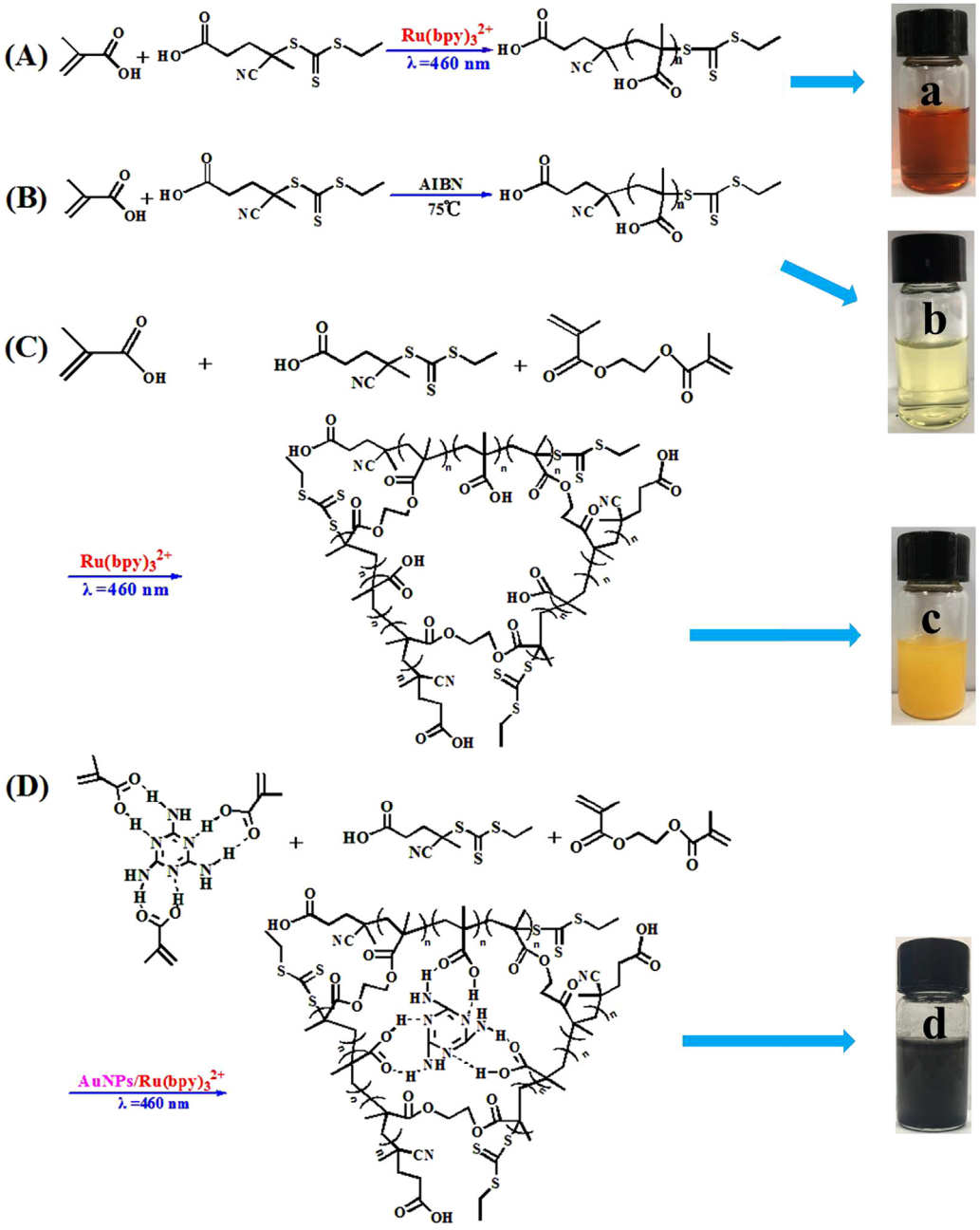

Scheme 2. (A) Synthesis of PMAA via Ru-PET-RAFT polymerization under visible light (λ = 460 nm) illumination. (B) Synthesis of PMAA via RAFT polymerization. (C) Synthesis of cPMAA via Ru-PET-RAFT cross-linking polymerization. (D) Synthesis of cPMAA using MEL as the template via Ru-PET-RAFT cross-linking polymerization. (a), (b), (c) and (d) represent digital photos of the aqueous solutions of the specified products.

polymerization, a set of control experiments were carried out. As indicated in Fig. 1B, no product was obtained without visible light illumination, which means that the presence of visible light was essential for inducing the polymerization. Besides, other polymerization conditions including the molar ratio of the MAA and RAFT agent as well as the amount of $Ru(bpy)_3^{2+}$ as well as the polymerization time were also studied. Compared with entries 1 and 2 of Table S1, it could be concluded that the RAFT agent and the photocatalyst $Ru(bpy)_3^{2+}$ were both essential for the PET-RAFT polymerizations. (Chen et al. 2016c) However, we also observed that the amount of $Ru(bpy)_3^{2+}$ had no obvious influence on the conversion of monomers in 12 h polymerization time when the concentration of $Ru(bpy)_3^{2+}$ is larger than 1.1×10^{-6} mol/L (Entries 3–5 and 8 of Table S1). Therefore, an optimal $Ru(bpy)_3^{2+}$ concentration (1.1×10^{-6} mol/L) was adopted in the following tests as shown in entries 6–11 of Table S1 to reduce the use of catalyst. The polymerizations with different [MAA]/[CETP] ratios in the same reaction time (12 h) indicated that the Mn of PMAA gradually enhanced with the enlarged molar ratios of monomer and RAFT agent (Entries 6–9). Furthermore, compared with Entry 8, Entry 10 and Entry 11, the prolongation of polymerization time had no significant effect on the conversion rate and Mn when the polymerization time was more than 24 h. Hence the optimum polymerization time was set at 24 h for the rest polymerizations.

In order to explore whether the polymerization was well-controlled or not, several typical characteristics of RAFT polymerization were also studied. Fig. S2A shows that the monomer conversion enlarged gradually with the prolongation of reaction time (empty rectangle, □). The filled rectangle indicate that the $\ln(M_o/M_t)$ and the polymerization time is in the pseudo-first order plot in the whole polymerization process, which shows that the concentration of free radicals is maintained

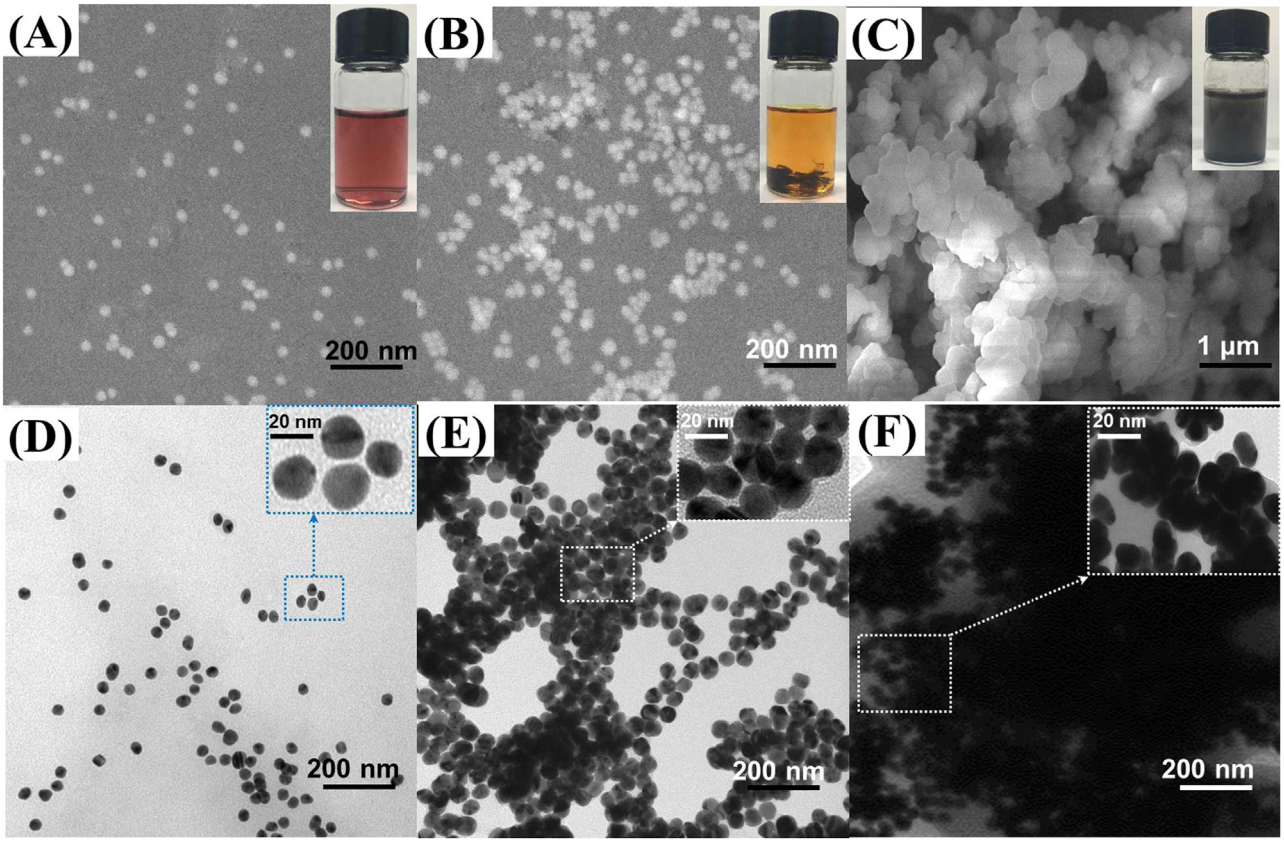

Fig. 2. (A) SEM images of AuNPs (B) TEM images of AuNPs. (C) the SEM images of Ru-AuNPs. (D) TEM images of Ru-AuNPs. (E) SEM images of AuNPs-MIPs and (F) TEM images of AuNPs-MIPs.

constant during the polymerization (filled rectangle, ■). Fig. S2B shows Mn and the Đs values at varying monomer conversion. It can be seen that the Mn of PMAA calculated from GPC method increases linearly with the increasing conversion (filled rectangle in Fig. S2B). In the meanwhile, the Mn of PMAA was calculated from the ^{1}H NMR spectra. It can be seen that the Mn values of PMAA obtained by GPC and ^{1}H NMR spectra were in a good agreement with theoretical ones (Fig. S2B and Table S2). GPC traces of PMAA obtained from different ratios of MAA to RAFT agent are exhibited in Fig. S2C. It could be concluded that the Mn (PMAA) is increased with the enlarged molar ratios of monomer (MAA) to RAFT agent. Besides, Đs of the obtained polymers were all less than 1.25, indicating the well-controlled RAFT mechanism (Table S1). All of these characterizations evidence the successful Ru-PET-RAFT polymerizations.

3.2. The characterizations of cPMAA via Ru-PET-RAFT cross-linking polymerization and the proposed mechanism

From the results above, $Ru(bpy)_3^{2+}$ has been confirmed as an efficient catalyst for PET-RAFT polymerization of MAA. Based on it, we tried to prepare cPMAA using MAA and EGDMA as the monomers and cross-linking agent. As shown in Scheme 2C, the cPMAA was prepared in the presence of visible light (λ = 460 nm) illumination at room temperature. Compared with the transparent solution of PMAA, the water solution of cPMAA was epinephelos and sedimentary. This is because the cross-linked copolymer of PMAA and EGDMA has much lower solubility. Then, the obtained cPMAA was analyzed by ^{1}H NMR. As shown in Fig. 1C the peaks at 3.50–3.10 ppm indicate the existence of the methylene groups which come from the cross-linking agent and the peaks at 12.20 ppm should be attributed to the carboxyl groups. The methyne and methylene groups on PMAA result in the peaks at 1.90 ppm and 1.2 ppm. Furthermore, the peaks at 8.90–5.50 ppm should result from $Ru(bpy)_3^{2+}$, which indicated that the prepared cPMAA still retained trace $Ru(bpy)_3^{2+}$. The content of carboxyl groups deceased due to the crosslinking of EGDMA with PMAA compared with the pure PMAA.

The obtained cPMAA was also characterized by FTIR spectra. As shown in Fig. 1D, the peaks at 3427 cm^{-1} and 3425 cm^{-1} can be assigned to the hydroxyl groups of PMAA and the peaks at 2924 cm^{-1} and 2881 cm^{-1} should be owing to the methylene groups as well as methyl groups of cPMAA, respectively. The characteristic peaks at 1750 cm^{-1} in FTIR spectrum of cPMAA was observed, which should be assigned to the C=O vibrational stretching from EGDMA and the –COOH groups from PMAA, Furthermore, we can observe that the peak signals of PMAA at the C=O vibrational stretching (the peaks at 1750 cm^{-1}) is greater than that of cPMAA, indicating that the PMAA has been successfully cross-linked by EGDMA. The major peaks at 3400–3100 cm^{-1} and 1650–1560 cm^{-1} should be assigned to the stretching vibration of C-H and telescopic vibration of aromatic heterocycle (pyridine of Ru $(bpy)_3^{2+}$). All of these results evidenced the successful preparation of cPMAA via Ru-PET-RAFT polymerization under visible light illumination at the wavelength of 460 nm.

A possible mechanism was proposed for the Ru-PET-RAFT controlled cross-linking polymerization. As illustrated in Fig. 1E, Ru $(bpy)_3^{2+}$ was used as photoredox catalyst to generate an excited $[Ru(bpy)_3^{2+}]^*$ in the presence of illumination (λ = 460 nm). Through PET process, $[Ru(bpy)_3^{2+}]^*$ can decay to the ground state $Ru(bpy)_3^{3+}$ and simultaneously reduce the RAFT agent (CETP), resulting in the production of radicals (Pn·). Pn· will lead to the copolymerization of the monomers with cross-linking reagent (MAA and EGDMA), and re-trigger the catalytic reaction cycle in the following polymerization process (Xu et al., 2014). The successful preparation of cPMAA further proved that Ru-PET-RAFT controlled cross-linking polymerization could provide a power tool for the synthesis of MIPs.

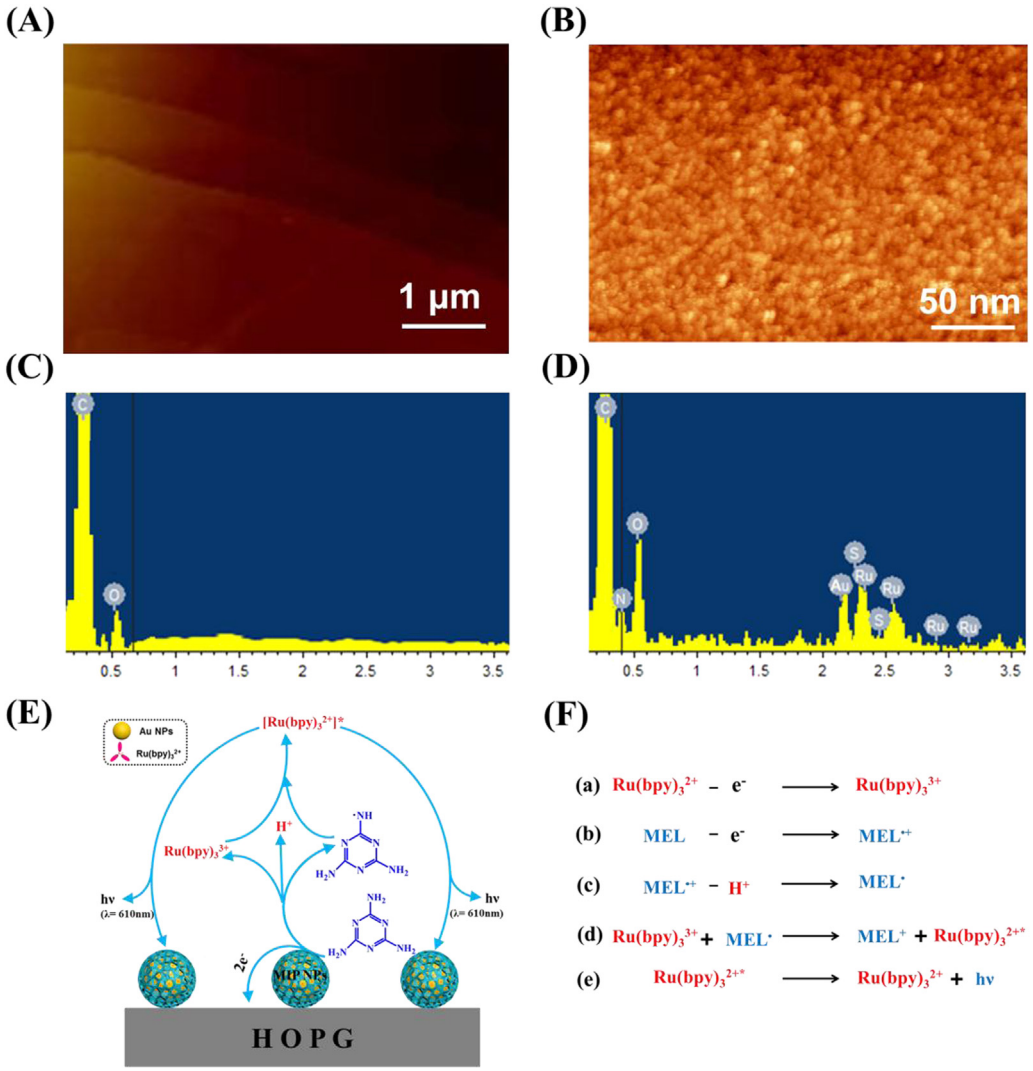

Fig. 3. (A) The AFM images of bare HOPG surface. (B) AFM image of MEL-MIPs-HOPG surface (C) EDS spectrum of bare HOPG (D) EDS spectrum of MEL-MIPs-HOPG. (E) and (F) possible mechanism for the ECL of MEL-$Ru(bpy)_3^{2+}$ system on HOPG surface.

3.3. The characterizations of AuNPs and AuNPs-MIPs

The SEM and TEM images of AuNPs show that most particles are nearly uniform and spherical with particle diameters of 20 nm (As shown in Fig. 2A and B), indicating the successful preparation of AuNPs via the reduction of $HAuCl_4$ in the presence of sodium citrate. The prepared AuNPs showed good dispersibility and stability, which can be attributed to electrostatic repulsion between the negatively-charged AuNPs. After the addition of $Ru(bpy)_3^{2+}$ into the AuNPs suspensions, the transparent and purple red solution (insert illustration of Fig. 2A) became orange and some black precipitate was produced (insert illustration of Fig. 2C). As shown in Fig. 2C and D, the obvious aggregation of AuNPs was observed, which should result from the electrostatic adsorption between the electronegative AuNPs and the electropositive $Ru(bpy)_3^{2+}$. Moreover, it also proved that $Ru(bpy)_3^{2+}$ had been successfully fixed on the surface of AuNPs. The particles size and morphology of AuNPs-MIPs were characterized by SEM. It could be observed from Fig. 2E that the as-prepared AuNPs-MIPs are in the form of clumps. The AuNPs-MIPs suspension was epinephelos and black in color as indicated in Scheme 2D(d) and the insert of Fig. 2E. From the TEM images (Fig. 2F), we could observe that the average size of AuNPs-MIPs was about 50 nm, which was consistent with the SEM results. The TEM images further evidenced that the AuNPs were successfully encapsulated by the MIPs.

3.4. Characterizations of the MEL-MIPs-HOPG and possible enhancement mechanism of the MEL-$Ru(bpy)_3^{2+}$ ECL system

AFM was utilized to characterize the bare HOPG and MEL-MIPs-HOPG surfaces. From Fig. 3A, we could observe that the bare electrode surface was smooth. As shown in Fig. 3B, the dense polymer brushes appeared when the MEL-MIPs were immobilized on the surface of HOPG. The EDS spectrum revealed that the bare HOPG surface mainly consists of carbon and oxygen. (Fig. 3C) When the MEL-MIPs were immobilized on HOPG, the EDS spectrum indicated the existence of N, S, Ru, Au and the augmented oxygen percentage on the electrode surface (Fig. 3D), indicating the successful immobilization of MEL-MIP on the HOPG electrode. EIS was also measured to characterize the changes of the HOPG surface before and after modification with MEL-MIPs. As shown in Fig. S3A(a), the electron transfer resistance (R_{et}) was measured to be 1860 Ω for the bare HOPG electrode. However, the R_{et} of the modified HOPG were obviously increased when MEL-MIPs were immobilized on the HOPG as shown in Fig. S3A(b). Moreover, it could be observed that the resistance of the MEL-MIPs-HOPG increased with the prolonged reaction time for the preparation of MEL-MIPs as shown in Fig. S3B. Accordingly, MEL-MIPs (12 h) was selected for the following study due to its smaller R_{et} (2490 Ω) and better electrical conductivity.

MEL can be used as a co-reagent for $Ru(bpy)_3^{2+}$ because the

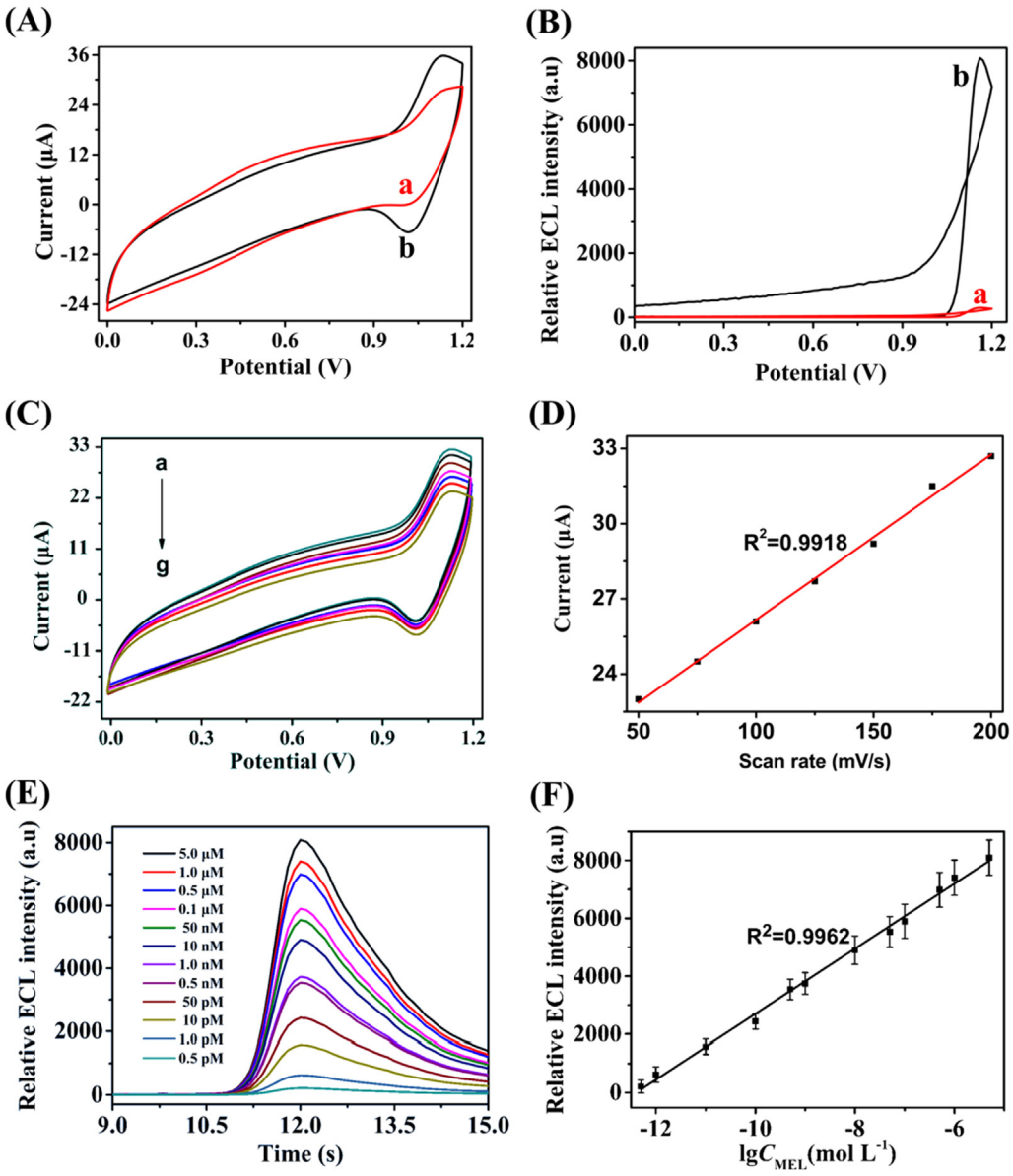

Fig. 4. (A) CVs and (B) the corresponding ECL intensity-potential curves for MEL-MIPs-HOPG in the absence (a) and presence (b) of 5 μM MEL in phosphate buffer solution (pH = 7.4) at the scan rate of 100 mV s^{-1}. (C) CVs of Ru-MIPs-HOPG at different scan rates: (a) - (g) are CV curves in 5 μM MEL phosphate buffer solution (PBS, pH = 7.4) at gradually decreased scan rates in the range 50–200 mV s^{-1}, . (D) The relationship between the anodic peak current and the scan rate. (E) The ECL intensities of MEL-MIPs-HOPG in 0.1 M PBS against different concentrations of MEL. (F) The linear fitting between the relative ECL intensity and the logarithm of the various MEL concentrations.

electron-donating groups (tertiary ammonia) of MEL could increase the ECL intensity due to the possible reaction mechanism between MEL and $Ru(bpy)_3^{2+}$. The possible mechanism is proposed as shown in Fig. 3E and F. (Chen et al., 2010; Liu et al., 2014) In details, MEL is oxidized to radical cation $MEL^{\bullet+}$ (Chen et al., 2015) in the meanwhile, $Ru(bpy)_3^{2+}$ undergoes a one-electron oxidation to produce $Ru(bpy)_3^{3+}$. The radical cation $MEL^{\bullet+}$ reduces $Ru(bpy)_3^{3+}$ to $[Ru(bpy)_3^{2+}]^*$, which can decay to the ground state $Ru(bpy)_3^{2+}$ through emitting luminescence. The radical cation $MEL^{\bullet+}$ is supposed to lose a proton to produce an intermediate $MEL^{\bullet}$. Therefore, MEL can effectively improve the ECL emission of $Ru(bpy)_3^{2+}$. The CVs and ECL of the MEL-MIPs-HOPG electrode were measured in the absence and presence of MEL. Fig. 4A shows that the presence of MEL led to the rise of anodic peak current and the decrease of cathodic peak current, which correspond with the mechanism of electrocatalytic reaction. (Zhou et al., 2014) We can clearly observe from Fig. 4B that the ECL response of $Ru(bpy)_3^{2+}$ enhanced sharply in the presence of 5 μM MEL and the intensity of ECL is nearly 24-fold higher than that without MEL, resulting from the co-initiator mechanism between MEL and $Ru(bpy)_3^{2+}$. All results demonstrate that a considerable amount of $Ru(bpy)_3^{2+}$ have been successfully immobilized onto the AuNPs surface. MEL could specifically pass through the MIPs and react with the fixed $Ru(bpy)_3^{2+}$ (Scheme 1C).

Fig. 4C shows the CVs of Ru-MIPs-HOPG in 0.1 M phosphate buffer at various scan rates. The oxidation peak at about 1.05 V could be observed from the redox wave, which should correspond to the typical redox reaction of $Ru(bpy)_3^{2+}$. (Dang et al., 2014; Guo et al., 2004) As indicated in Fig. 4D, the anodic peak current is in proportion to scan rate within the range of 50–200 mV s^{-1}, proving that the ECL behavior of $Ru(bpy)_3^{2+}$ is a surface-controlled process. (Wang et al., 2009) The ECL intensities of Ru-MIPs-HOPG sensor at different concentrations of MEL from 5 μM to 0.5 pM were measured. As shown in Fig. 4E, the increasing intensity of ECL was accompanied by increasing MEL content in the PBS. The Fig. 4F shows that the ECL intensity exhibited a linear response to the logarithmic MEL concentration in the range from 5 μM to 0.5 pM with a correlation coefficient of 0.9962, while a low detection limit of 0.1 pM was obtained. Moreover, recovery studies were also carried out for real milk samples. There was no obvious MEL detected in the pretreated milk samples. Then, the samples were studied with a standard-addition method by adding a certain amounts of MEL (5.0×10^{-13} M, 5.0×10^{-10} M, 5.0×10^{-6} M) to the pretreated milk samples. The obtained results of the as-prepared sensor are shown in

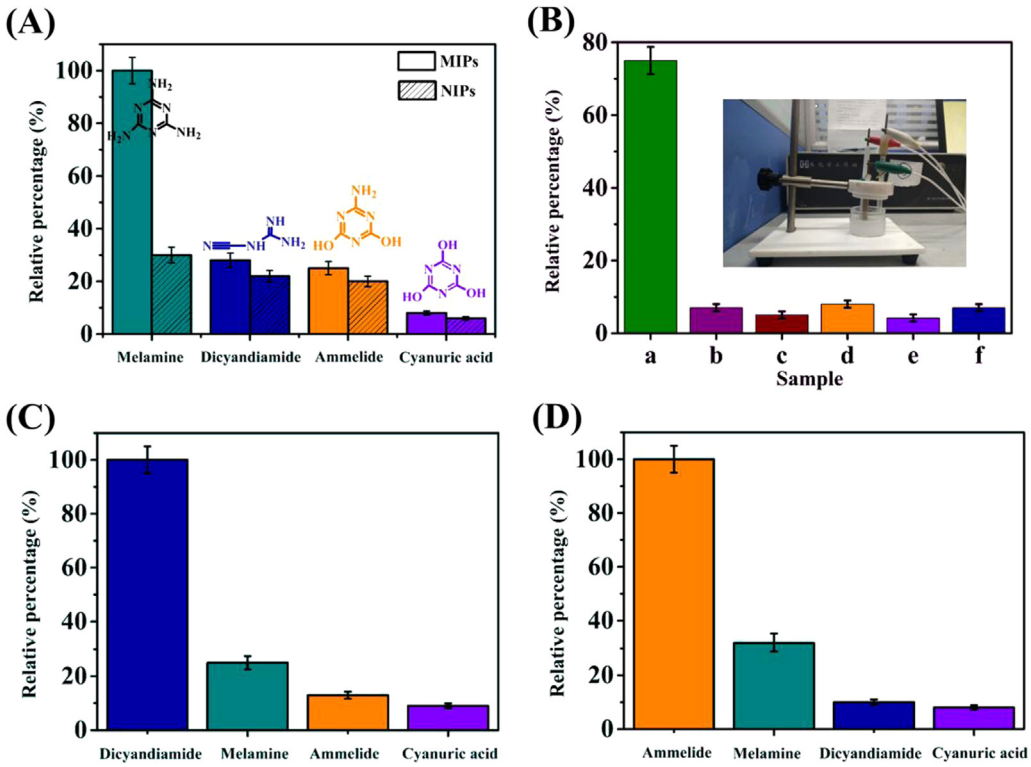

Fig. 5. (A) Selectivity test of the MEL-MIPs-HOPG sensors to MEL, dicyandiamide, ammelide, and cyanuric acid, where the concentrations of these samples were 5 μM. (B) The detection of MEL in real milk samples. Samples b-f were milk samples (10 mg/mL in PBS) from different suppliers. Sample a was obtained by adding 0.15 mg/L MEL into Sample b. (C) and (D) the relative ECL intensity of dicyandiamide-MIPs-HOPG/ammelide-MIPs-HOPG in different solutions, respectively. The concentrations of these samples were 5 μM.

Table S3, and the recoveries were found to be 98.4%, 99.8%, 101%, respectively. Compared with the previous work (Table S4), the as-prepared ECL sensor shows a wider detection range and a comparable lowest detection limit, which is mainly due to good conductivity and large surface area of the AuNPs, which can load a large amount of Ru $(bpy)_3^{2+}$ probes. Besides, the LSPR phenomenon of AuNPs (Wang et al., 2015a) could also effectively enhance the ECL emission of $Ru(bpy)_3^{2+}$ and thus apparently increase the sensitivity of the sensors.

3.5. Selectivity test of the developed MEL-MIPs modified sensor

The specific recognition ability of MEL-MIPs-HOPG was further implemented to study the selectivity of the as-prepared sensor. As shown in Fig. 5A, when the ECL response intensity to MEL concentration (5 μM) was set to 100%, those to dicyandiamide, ammelide and cyanuric acid at the same concentration were 28%, 25%, and 17%, respectively, which are much lower, indicating the good selectivity of MEL-MIPs-HOPG towards MEL. Moreover, the ECL response of NIPs-HOPG was lower than that of MEL-MIPs-HOPG, because there is no specific recognition site in the structure of NIPs. In order to explore the effectiveness of MEL-MIPs-HOPG in practical applications, we detected the actual milk samples as shown in Fig. 5B. It should be noted that the milk Samples a-f (10 mg/mL in PBS) were bought from different manufacturers. Sample a was obtained by adding 0.15 mg/L MEL (the highest concentration allowed in dairy products stipulated by Food and Agriculture Organization of the United Nations (Ritota and Manzi, 2018) to Sample b. Impressively, Samples b-f showed weak ECL response while Sample a exhibited obviously higher ECL intensity. These results proved that the MEL contents in both Samples a-f were lower than the regulated standards and the as-prepared sensors showed a satisfied sensitivity in practical applications.

3.6. Reusability and long-term stability tests of the sensors

Cyclic stability of the MEL-MIPs ECL sensors was investigated via uninterrupted CV scanning for 112 cycles in 3000 s with 10 μM MEL (As shown in Fig. S4A). The maximum relative standard deviation of the ECL intensity was calculated to be 0.71%, proving the good stability and repeatability of the ECL sensor. To test the long-term stability, ECL intensity of the sensor was collected in 10 μM MEL every ten days, during the 90-day storage time. As indicated in Fig. S4B, the ECL intensity of the constructed sensor slightly decreased in the first 50 days and then remained stable in the following 40 days, which demonstrated that the as-prepared solid-state ECL sensor showed good long-term stability. Its good reusability and long-term stability should be due to the stable fixation of electropositive $Ru(bpy)_3^{2+}$ on electronegative AuNPs via electrostatic attraction, which avoided the falling off of ECL probes ($Ru(bpy)_3^{2+}$) from the ECL sensors.

3.7. Universality test of the proposed platform

In order to confirm the universality of the proposed strategy, MIPs-HOPG using other MEL structural analogues as the templates was also prepared. As shown in Fig. 5C, the dicyandiamide-MIPs-HOPG sensor shows a higher specific recognition ability to dicyandiamide compared to MEL and ammelide. Similarly, the ammelide-MIPs-HOPG also displays the specific recognition ability to ammelide (Fig. 5D). All these results indicate that we have established a versatile ECL sensing platform with specific recognition ability for detection of a variety of substances.

4. Conclusions

In present work, we have successfully synthesized PMAA and cPMAA via well-controlled Ru-PET-RAFT and Ru-PET-RAFT cross-linking polymerizations, respectively. Taking advantage of the combinative merits of this new polymerization method and ECL techniques as well as MIT, a versatile and effective ECL sensing platform was successfully constructed using bifunctional ruthenium complex as both the catalyst and sensing probes. The as-prepared sensor exhibited benign sensitivity, good reusability, satisfied long-term stability and excellent specific recognition ability, which were better or comparable to the

previously reported performances. More importantly, this sensing platform could be utilized for detection of MEL in real samples with good performance. Besides, it could be anticipated that the gentle reaction condition of the proposed Ru-PET-RAFT cross-linking polymerization could provide a powerful tool for preparation of MIPs using vulnerable biomolecules as the templates such as enzymes and DNA. However, only the targets with tertiary amine groups could be detected using $Ru(bpy)_3^{2+}$ as the sensing probes due to the specific reaction mechanism, which may limit the universality of the sensor. All in all, the proposed strategy for fabricating MIP-ECL sensors might envision potential applications in biological recognition, protein detection and environmental risk monitoring, etc.

Acknowledgements

This work was supported by Qingdao Innovation Leading Talent Program, Qingdao (12-1-4-2-2-jch) and Taishan Scholars Program.

Appendix A. Supporting information

Supplementary data associated with this article can be found in the online version at doi:10.1016/j.bios.2018.09.083.

References

Ai, K., Liu, Y., Lu, L., 2009. J. Am. Chem. Soc. 131, 9496–9497.
Bertoncello, P., Forster, R.J., 2009. Biosens. Bioelectron. 24, 3191–3200.
Cai, H.H., Yu, X., Dong, H., Cai, J., Yang, P.H., 2014a. J. Food Eng. 142, 163–169.
Cai, X., Li, J., Zhang, Z., Yang, F., Dong, R., Chen, L., 2014b. ACS Appl. Mater. Interfaces 6, 305–313.
Cakir, P., Cutivet, A., Resmini, M., Bui, B.T., Haupt, K., 2013. Adv. Mater. 25, 1048–1051.
Cao, Y., Xu, Y., Zhang, J., Yang, D., Liu, J., 2015. Polymer 61, 198–203.
Chen, L., Xu, S., Li, J., 2011. Chem. Soc. Rev. 40, 2922–2942.
Chen, L., Wang, X., Lu, W., Wu, X., Li, J., 2016a. Chem. Soc. Rev. 45, 2137–2211.
Chen, T., Han, X., Peng, Z., Li, A., Liu, J., 2016a. Eur. Polym. J. 81, 327–336.
Chen, T., Xu, Y., Peng, Z., Li, A., Liu, J., 2016b. Polym. Chem.-Uk. 7, 5880–5887.
Chen, X., Lian, S., Ma, Y., Peng, A., Tian, X., Huang, Z., 2015. Talanta 146, 844–850.
Chen, T., Xu, Y., Yang, W., Li, A., Wang, Y., Sun, J., Liu, J., 2018a. Macromol. Biosci. 18, 1700312.
Chen, X., Liu, Y., Ma, Q., 2018b. J. Mater. Chem. C 6, 942–959.
Chen, X.M., Cai, Z.M., Lin, Z.J., Jia, T.T., Liu, H.Z., Jiang, Y.Q., Chen, X., 2009. Biosens. Bioelectron. 24, 3475–3480.
Chen, X.M., Wu, G.H., Chen, J.M., Jiang, Y.Q., Chen, G.N., Oyama, M., Chen, X., Wang, X.R., 2010. Biosens. Bioelectron. 26, 872–876.
Cheng, H.W., Chen, Y.Y., Lin, X.X., Huan, S.Y., Wu, H.L., Shen, G.L., Yu, R.Q., 2011. Anal. Chim. Acta 707, 155–163.
Chester, T.L., 2013. Anal. Chem. 85, 579–589.
Dang, J., Guo, Z., Zheng, X., Chem, A., 2014. Anal. Chem. 86, 8943–8950.
Feng, Y., Sun, F., Wang, N., Lei, J., Ju, H., 2017. Anal. Chem. 89, 7659–7666.
Fu, C., Xu, J., Tao, L., Boyer, C., 2014. ACS Macro. Lett. 3, 633–638.
Gillette, M.A., Carr, S.A., 2013. Nat. Methods 10, 28–34.
Gomez, L.P., Spangenberg, A., Ton, X.A., Fuchs, Y., Bokeloh, F., Malval, J.P., Tse, S.B.B., Thuau, D., Ayela, C., Haupt, K., 2016. Adv. Mater. 28, 5931–5937.
Guo, S., Wen, D., Zhai, Y., Dong, S., Wang, E., 2010. ACS Nano 4, 3959–3968.
Guo, Z., Dong, S., Chem, A., 2004. Anal. Chem. 76, 2683–2688.
He, Y., Huang, Y., Jin, Y., Liu, X., Liu, G., Zhao, R., 2014. ACS Appl. Mater. Interfaces 6, 9634–9642.
Li, D.Y., He, X.W., Chen, Y., Li, W.Y., Zhang, Y.K., 2013. ACS Appl. Mater. Interfaces 5, 12609–12616.
Li, H., Chen, J., Han, S., Niu, W., Liu, X., Xu, G., 2009. Talanta 79, 165–170.
Li, X., Zhang, B., Li, W., Lei, X., Fan, X., Tian, L., Zhang, H., Zhang, Q., 2014. Biosens. Bioelectron. 51, 261–267.
Liu, F., Gao, Y., Li, W., Shao, J., 2014. RSC Adv. 4, 34003–34007.
Liu, F., Yang, X., Sun, S., 2010a. Analyst 136, 374–378.
Liu, J., Setijadi, E., Liu, Y., Whittaker, M.R., Boyer, C., Davis, T.P., 2010b. Aust. J. Chem. 63, 1245–1250.
Lu, L.M., Zhang, L., Qu, F.L., Lu, H.X., Zhang, X.B., Wu, Z.S., Huan, S.Y., Wang, Q.A., Shen, G.L., Yu, R.Q., 2009. Biosens. Bioelectron. 25, 218–223.
Miao, W., 2008. Chem. Rev. 108, 2506–2553.
Miao, Y., Wen, Y., Dong, J., Zhou, W., Zhang, Z., Yang, H., 2011. Biosens. Bioelectron. 26, 2994–2999.
Nasiri, K.Y., Sun, S., 2017. Chem. Commun. 53, 9042–9054.
Nie, W., Wang, Q., Yang, X., Zhang, H., Li, Z., Gao, L., Zheng, Y., Liu, X., Wang, K., 2017. Anal. Chim. Acta 993, 55–62.
Qian, J., Wang, K., Jin, Y., Yang, X., Jiang, L., Yan, Y., Dong, X., Li, H., Qiu, B., 2014. Biosens. Bioelectron. 57, 149–156.
Ritota, M., Manzi, P., 2018. Food Anal. Method. 11, 128–147.
Schirhagl, R., 2014. Anal. Chem. 86, 250–261.
Tao, C., Xu, Y., Zhi, P., Li, A., Liu, J., 2017. Anal. Chem. 89, 2065–2072.
Uzun, L., Turner, A.P.F., 2015. Biosens. Bioelectron. 76, 131–144.
Wang, D., Guo, L., Huang, R., Qiu, B., Lin, Z., Chen, G., 2015a. Sci. Rep. 5. https://doi.org/10.1038/srep07954.
Wang, D., Li, Y., Lin, Z., Qiu, B., Guo, L., 2015b. Anal. Chem. 87, 5966–5972.
Wang, K., Hua, Y., Lin, Z., Ma, Z., Xing, S., Qiang, L., Liao, J., Liu, C., Wei, X., 2009. Electrochim. Acta 54, 4626–4630.
Wang, X., Rui, X., Xu, S., Wang, Y., Xiang, R., Du, B., Dan, W., Qin, W., 2017. Biosens. Bioelectron. 96, 239–245.
Wang, Z., Ma, X., Zhang, L., Yang, W., Gong, L., He, P., Li, Z., 2010. Anal. Chim. Acta 662, 69–75.
Wei, F., Lam, R., Cheng, S., Lu, S., Ho, D., Li, N., 2010. Appl. Phys. Lett. 96. https://doi.org/10.1063/1061.3373325.
Wei, H., Wang, E., 2008. Trac-Trend Anal. Chem. 27, 447–459.
Weissman, S.J., Adler, A., Qin, X., Zerr, D.M., 2015. Biosens. Bioelectron. 67, 595–600.
Wu, B., Hu, C., Hu, X., Cao, H., Huang, C., Shen, H., Jia, N., 2013. Biosens. Bioelectron. 50, 300–304.
Xing, H., Zhai, Q., Zhang, X., Li, J., Wang, E., 2018. Anal. Chem. 90, 2141–2147.
Xu, J., Jung, K., Boyer, C., 2014. Macromolecules 47, 4217–4229.
Xu, L.J., Lei, Z.C., Li, J., Zong, C., Yang, C.J., Ren, B., 2015. J. Am. Chem. Soc. 137, 5149–5154.
Xu, S., Lu, H., 2015. Biosens. Bioelectron. 73, 160–166.
Xu, Z., Yu, J., 2010. Nanotechnology 21. https://doi.org/10.1088/0957-4484/1021/1024/245501.
Yin, J., Cui, Y., Yang, G., Wang, H., 2010. Chem. Commun. 46, 7688–7690.
Zhang, L., Li, J., Xu, Y., Zhai, Y., Li, Y., Wang, E., 2009. Talanta 79, 454–459.
Zhang, Y., Li, L., Zhang, L., Ge, S., Yan, M., Yu, J., 2017. Nano Energy 31, 174–182.
Zhao, F., Zeng, J., Parvez Arnob, M.M., Sun, P., Qi, J., Motwani, P., Gheewala, M., Li, C.H., Paterson, A., Strych, U., 2014. Nanoscale 6, 8199–8207.
Zhou, X., Zhu, D., Liao, Y., Liu, W., Liu, H., Ma, Z., Xing, D., 2014. Nat. Protoc. 9, 1146–1159.